Applied Physics A (2020) 126:59
https://doi.org/10.1007/s00339-019-3258-5

Applied Physics A
Materials Science & Processing

Opto-structural properties of Si-rich SiN_x with different stoichiometry

F. Tiour[1,2] · B. Benyahia[2] · N. Brihi[1] · A. Sari[3] · Br. Mahmoudi[2] · A. Manseri[2] · A. Guenda[2]

Received: 29 September 2019 / Accepted: 21 December 2019 / Published online: 1 January 2020
© Springer-Verlag GmbH Germany, part of Springer Nature 2020

Abstract

This study deals with the fabrication and characterization of silicon nanoparticles in a SiN_x dielectric matrix to have thin films of different gap energies, films essentially based on silicon. Hydrogenated silicon-rich nitride films SiN_x:H with different stoichiometry $X=N/Si$ were grown on Si substrate using industrial low-frequency plasma-enhanced chemical vapor deposition (LF-PECVD). Optical, electrical, and structural properties of the obtained films have been studied after rapid thermal annealing at 950 °C. The GIXRD and Raman analysis demonstrate that the films contain simultaneously the hexagonal β-Si_3N_4 phase and crystalline silicon nanoparticles and the average size of silicon nanocrystallites is within the range of 2.5–11 nm according to the stoichiometry. A strong visible photoluminescence (PL) can be observed in silicon nitride and the evolution of PL with the NH_3/SiH_4 ratio is correlated with the evolution of the structure. The layers having a luminescence in the visible region present a photocurrent (PC) in the high-energy region. PC spectroscopy has clearly demonstrated the existence of increased absorption on the high-energy side associated with Si-Ncs and confirms the potential of Si-Ncs for photovoltaic applications.

Keywords SiNx:H · Plasma-enhanced chemical vapor deposition (PECVD) · Si nanocrystals (Si-Ncs) · X-ray diffraction · Photoluminescence

1 Introduction

Several domains have exploited the properties of silicon nanocrystals (Si-Ncs) embedded in dielectric matrix for different applications [1–6]. In electronic, the location properties of the -charges have been used for the production of nonvolatile memories [2]. In the field of optoelectronics, nanoparticles offer the possibility of modifying the emission wavelength and significant increase in the radiative emission efficiency. For electroluminescence devices, the characterization of retention time for conversion of optical on–off keying data (short carrier recombination time within Si-QDs embedded in SiN_x LED) [7] and decrease the turn-on voltage of Electroluminescent diodes based on nanostructured silicon have also been improved [8, 9]. In microelectronic and to enhance the efficiency of the next-generation integrated circuit, intense research is being in data processor where the wavelength conversion-based optical Kerr switch has been demonstrated [10]. However, the absorption of such a structure is significantly increased and it is imaginable to change the wavelength range absorbed in solar cell devices [4-6]. In this regard, many research avenues exist to improve the competitiveness of photovoltaic energy compared to conventional energies. Among them, Si-rich silicon nitride film-embedded silicon nanocrystals (Si-Ncs) are at the heart of many third-generation photovoltaic concepts (spectral shift, tandem cells…). [1, 11, 12]. SiN_x is a preferred dielectric matrix in view of its high charge-trapping ability and high carrier mobility due to its improving dielectric and electroluminescent properties. A control of the nanoparticles as well as the matrix which encompasses them is essential to consider their application.

Silicon nitride (SiN_x) thin dielectric films are now widely used as an antireflection and passivation layer in crystalline silicon cells. The idea of using the SiN_x matrix as host matrix for silicon nanoparticles has been proposed by several

✉ F. Tiour
tiourfaiza@yahoo.fr

[1] Faculty of Sciences, Mohamed Seddik BenYahia University, Jijel, Algeria

[2] Research Center in Semiconductor Technology for Energy, 02, Bd. Frantz Fanon, BP. 140 Alger 7 Merveilles, Algiers, Algeria

[3] Laboratory of Post-Irradiation Control of Nuclear Materials, Nuclear Research Center, Birine, Djelfa, Algeria

authors [13–15]. The goal is to make the active layer and thus to add value to the antireflection layer conventionally used for silicon-based photovoltaic cells, because this approach would be directly transferable to the photovoltaic industry.

One solution for conserving low production costs is to use Si-Ncs embedded in a dielectric matrix obtained by thin film deposition techniques. The control of the gap energy could be obtained by controlling the size of these Si-Ncs, and the dielectric matrix. This would be the key parameter to adjust the absorption of the thin layer. Conduction properties would depend on the matrix in which the Si-Ncs are integrated.

Jiang et al. [16] have estimated that to obtain sufficient conduction properties, the distance between two nanoparticles must be at most 1–2 nm for SiO_2, while for SiN_x, the distance could be between 2 and 4 nm. Thus, the conduction between the nanoparticles can be significantly increased if the potential barrier decreases, thanks to the use of a silicon nitride matrix.

In the photovoltaic industrial sector, LF-PECVD reactors are widely used. This is the case of our reactor developed by SEMCO Engineering. Since SiN_x is widely used as an antireflection layer for silicon solar cells, a first approach would be to make this material active in photo-generation and carrier-collection processes. It would be interesting to test the potential contribution of these silicon nanocrystals embedded in the antireflection coating (ARC) for conventional silicon photovoltaic cells without modifying the basic manufacturing process of the solar cells.

In this paper, we describe the fabrication and we studied and optimized growth conditions PECVD silicon nitride enriched with silicon nanoparticles with reference to the results of the structural characterization and we investigate the effects of the microstructure on the absorption and photocurrent properties by optic and electro-optic spectroscopy of these nanomaterial. At first, the conditions of formation of these nanostructures in nitride layers enriched in silicon deposited by PECVD are studied to find the optimum conditions for deposition having a high density of nanoparticles with a controlled size.

2 Experimental

We used 4-inch Cz, (100) silicon wafers, 450 µm thick, p-type (boron doped), 0.5–2.5 Ωcm in resistivity. The saw damage was first removed in a hot NaOH solution. This was followed by cleaning in HCl and a final dip in dilute HF prior to the diffusion process. A doped n + emitter was realized by diffusion at 920°c using a liquid POCl3 source [17]. SiN_x films were deposited in an industrial direct plasma pulsed reactor operating at low frequency using a mixture of silane (SiH_4) and ammonia (NH_3). The chemical composition of the layers was controlled by the gas flow ratio $R = NH_3/SiH_4$ ranging between 0.5 and 6. The fixed processing parameters were a temperature of 380°c, tube pressure 1700 mmHg. All the experiments were conducted at a constant power of 4.6 KW.

Rapid Thermal annealing (RTA) at 950°c for 70 s in flowing nitrogen was applied to produce the Si-Ncs in the films. Since previous work has shown that the SiN_x layer has an amorphous character without annealing [21].

Rutherford Backscattering Spectrometry (RBS) analysis was employed to determine the nitrogen and silicon composition of the films. We used the RBS particle-induced X-ray emission (PIXE). The measurements were carried out at room temperature using a 2 MeV 4He + ion beam with an incident normal direction to the surface sample. The backscattered ions were collected at a scattering angle of 160°. The RBS spectra were analyzed using the SIMNRA code.

The refractive indices and the thicknesses were controlled by an ellipsometer DRE ELX-02 C DRE single wavelength (632.8 nm) using a He–Ne laser beam.

Grazing incidence X-ray diffraction was employed to investigate the crystal structure of annealed samples using an X'Pert Pro MPD diffractometer with Cu-K_α (1.5408 angström) radiation source. The GIXRD patterns of all samples were acquired with a step size of 0.026°, time per step of 85 s and 2θ range from 20 to 90°. The angle of incidence ω was set to 1.5°. Raman spectroscopy technique was used to identify the structure, amorphous or crystalline, of Si nanoclusters in the films. Raman spectra were recorded at room temperature, using the LabRAM HR Evolution Horiba Raman spectrometer. A 325 nm laser line was used as a source.

PL spectra were recorded between 200 and 700 nm using an UV light from a Xenon lamp as the excitation source from a Perkin Elmer LS-50B luminescence spectrometer.

The electrical measurements for each incident wavelength were carried out to evaluate the contribution of Si-Ncs to the photocurrent of Si solar cells. They have been acquired using a Jobin–Yvon H25 monochromator with a tungsten filament lamp by an incident power of 170 W under PC control and chopped monochromatic excitation light for a synchronous detection. The light flux was measured using a calibrated photodiode.

3 Result and discussion

3.1 Content and composition analysis

Figure 1 shows an example of RBS spectrum of a SiN_x layer with red simulation spectrum by SimNRA computer code. The simulation reproduces correctly the experimental signal of the sample.

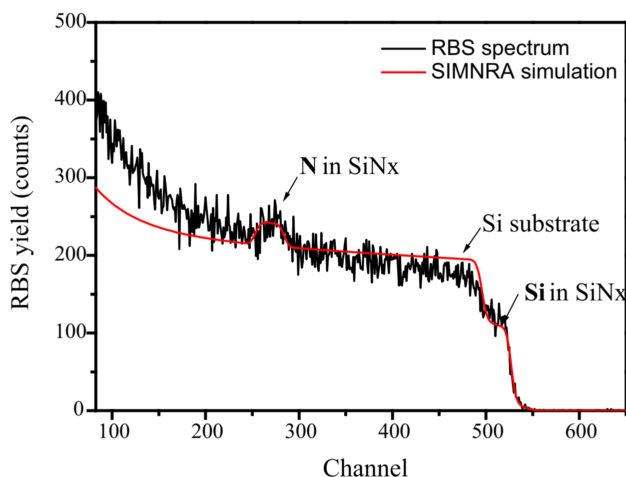

Fig. 1 Typical RBS spectrum of a SiNx layer as deposited

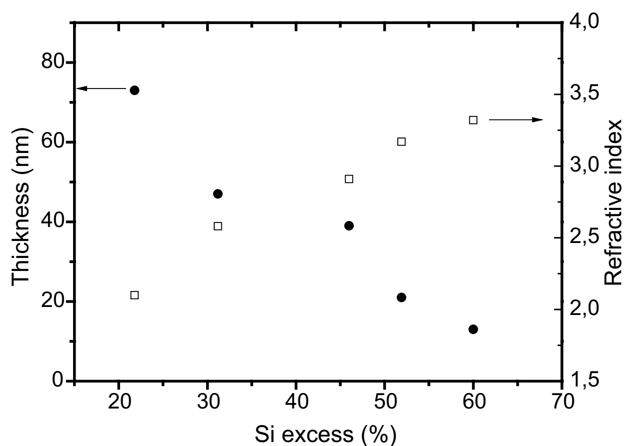

Fig. 2 Evolution of the refractive index and thickness of SiNx thin films as a function of Si excess

RBS analyzes was used to determine the nitrogen and silicon composition of the films. The atomic chemical compositions quantified are reported in Table 1. The stoichiometry of as-deposited films can be determined as $x = [N]/[Si]$. The excess silicon is estimated from the atomic composition. The excess Si content was estimated as $[Si_{excess}] = ((4-3x)/(4+4x)) \times 100\%$ [18].

High excess silicon in a silicon nitride matrix containing no oxygen is obtained.

The layers made with a low ratio $NH_3/SIH_4 = 0.5$ are rich in silicon, an excess of 60 at% is estimated. By increasing the value of NH_3/SIH_4 (i.e. the ammonia flow), the percentage of excess Si in the layer decreases rapidly. Beyond $NH_3/SIH_4 = 6$ deposited SiN_x layers are stoichiometric.

With the control of gas flow, it will be possible to control the chemical composition of SiN_x layers.

Ellipsometric measurements were performed for the SiN_x layers having different excess silicon. We determined the optical parameter, refractive index (n), and thicknesses of these SiN_x layers at 632.8 nm. Figure 2 shows the results of the ellipsometry analysis of these samples containing Si excess levels between 60 and 22%.

As the gas flow ratio is decreased, the refractive index increases. The refractive index varies from 2.0, typical of stoichiometric PECVD hydrogenated silicon nitride [19] to 3.3, characteristic of silicon-rich silicon nitride, thus supporting increasing silicon content in the films [20]. As the ammonia level increases, the quantity of material arriving at the growing film also increases. This could be one of the reasons why the film thickness is also increasing as it is observed on Fig. 2.

Table 1 Chemical composition of SiNx layers obtained by varying the gas flow ratio R between 0.5 and 6

$R = (NH_3/SiH_4)$	%at. Si	%at. N	Si excess (%at.)
0.5	65	19.2	60
2	60.8	23	51.9
3	58	25.8	45.8
4	52	33.7	31.2
6	48.9	39.5	21.8

3.2 Structural properties

To better understand the microstructure of the SiN_x films, GIXRD was used to reveal information about the crystallographic structure and to verify the nanocrystals formation. All deposited layers were amorphous at the deposition temperature which has been verified in previous work [21].

Usually, XRD is applied to powder samples and the thin-film structures investigated in this study have reduced crystalline volume and, therefore, require glancing incidence X-ray diffraction (GIXRD) to maximize the path length in the sample. All values are presented as approximate values to show comparative changes in the size of the nanocrystals with NH_3/SiH_4 ratio.

In the GIXRD configuration, X-ray penetration depth is controlled by fixing the incident angle. The angle of incidence was judiciously selected just above the critical angle tolerating the X-ray penetration depth to be adjacent to the film thickness, even if a weak additional contribution from the substrate appears.

For the specific study of these thin films (80 nm max.), the intensity of the diffracted signal coming from the substrate Si (400) is strongly reduced.

In Fig. 3, the evolution of the GIXRD pattern of the 950 °C annealed films with NH_3/SIH_4 is shown. The samples whose ratio are in the range 0.5–3 show a few broad peaks with a broad envelope peak, which underlies the

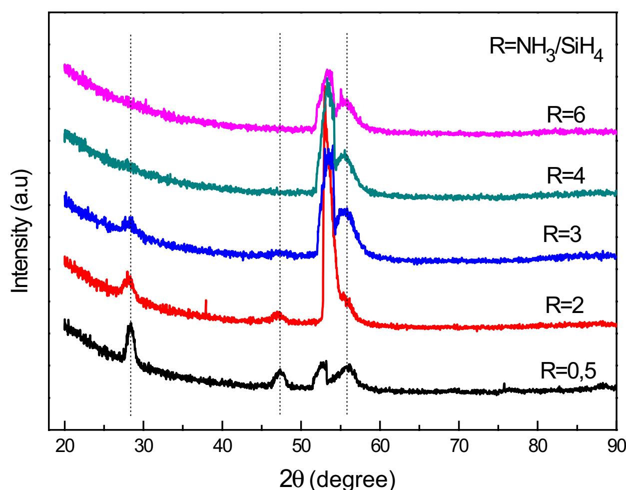

Fig. 3 The GIXRD patterns for annealed samples depend on the Si content given by ratio NH_3/SiH_4

Bragg peaks, indicating that two phases, crystalline and amorphous, coexist in the same sample. The spectra clearly exhibit the formation of broadened silicon (111), (2 2 0), and (311) peaks, in conformity with the database (33–1160), confirming that silicon crystallization occurs in silicon nitride. Moreover, the broad diffraction peak resulting from the overlap of two peaks identified at $2\theta = 51.8°$ and 52.5° suggest incomplete crystallization of silicon nitride α and β-Si_3N_4 nanocrystals, the most common polymorphs of crystalline silicon nitride according to the crystallographic letters [01-076-1409] and [01-082-0702], respectively.

The determination of crystallite size from the Scherrer's formula requires a flat baseline. After subtracting the baseline, Fig. 4 shows that the peaks have a better signal/noise.

As can be observed, the X-ray diffraction pattern corresponding to the film grown at $NH_3/SIH_4 = 0.5$ ($SiN_{0.30}$) show

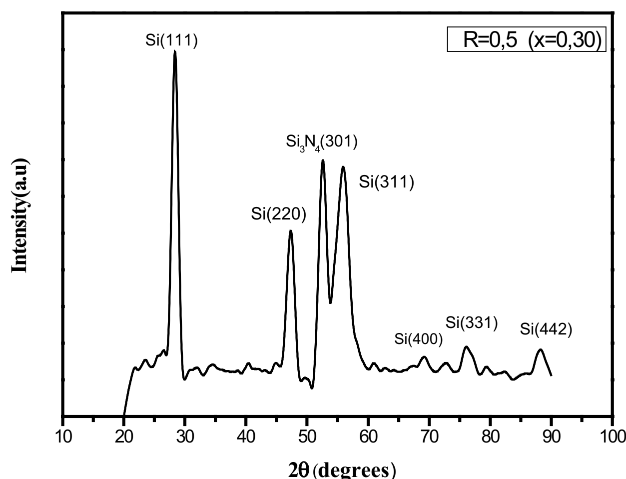

Fig. 4 The GIXRD pattern for annealed SiNx film ($NH_3/SiH_4 = 0.5$)

six predominant c-Si peaks along (111), (220), (311), (400), (331) and (442) [22].

The observed values which correlate with the Si phase data reported in JCPDS database (33–1160) reference, shown in Table 2, indicate close match within ± 0.1∘of 2*θ* values. The data correspond well with the reported values in the literatures and prove the presence of Si-Ncs in the film.

The GIXRD analysis was also used to measure the average particle size from FWHM of the dominant peak at 28.35∘ using Debye–Scherer formula [22].

$$L = \frac{0.94\lambda}{B(2\theta)\cos(\theta)}, \quad (1)$$

where λ is the wavelength of the X-ray beam (Cu K_α, 1.5406 Å), B (2θ) is the full-width at half-maximum (FWHM) of the diffraction peak (in radian) and θ is the diffraction angle.

According to Scherer's formula, the average crystallite size range of nanocrystalline silicon for each composition is shown in the first column in Table 3. Noting that, the GIXRD spectrum represents the deconvolution of all silicon crystallites diffraction with various sizes. Thus, these values represent the average size of the dominant crystallites in the film.

Figure 5 presents the Raman spectrum of SiN_x films with various NH_3/SIH_4 values. It is seen that the evolution of the Raman spectra depends on the composition.

All spectra show the dominant peak centered at approximately 521 cm^{-1} which is attributed to the transverse optical (TO) mode of Si–Si vibrations in the crystalline phase [23]. Furthermore, three regions of amorphous silicon, i.e. (140 cm^{-1}, 300 cm^{-1}, 480 cm^{-1}) which, respectively, correspond to the transverse acoustic branch (TA), longitudinal acoustic model (LA) and transverse optical model (TO_a) [24, 25]. Besides, the formation of a crystalline Si phase is also consistent with the appearance of a weak peak at 430 cm^{-1}, that is attributed to the second order of the transverse acoustic (2TA) phonon mode [25].

It is observed that the intensity of the (TA) and (LA) mode (at 140 cm^{-1} and 300 cm^{-1}) increases with the decreasing NH_3/SIH_4 that gives an evidence about the medium-range order of amorphous network in the thin films containing

Table 2 JCPDS and observed data

2 (JCPDS)	2 (observed)	hkl
28.44	28.35	111
47.30	47.35	220
56.12	56.09	311
69.13	69.21	400
76.37	76.30	331
88.03	88.31	442

Table 3 Evolution of the Si-Ncs size as a function of the ratio ($R=NH_3/SiH_4$) obtained by XRD and calculated from different simulated equations

950 °C	Average crystallite size range by XRD [Å]	Crystallite size[Å] estimated by [49]	Crystallite size[Å] estimated by [50]	Crystallite size[Å] estimated by [41]
$R=0.5$	55–110	47–60	40–50	45–65
$R=2$	40–70	30–60	30–50	40–55
$R=3$	35–50	30–35	31–33	40–45
$R=4$	25–40	22–34	24–31	32–45

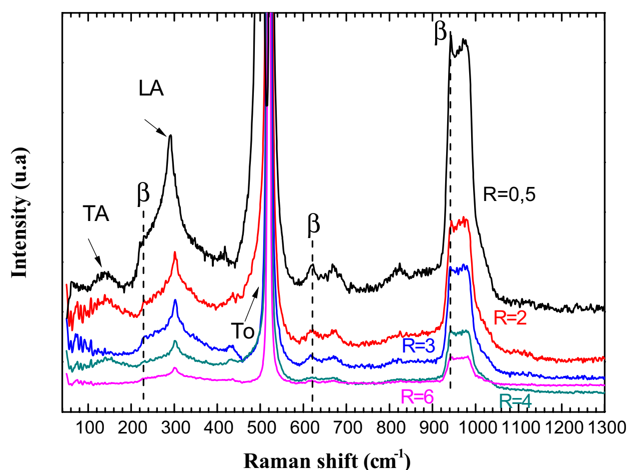

Fig. 5 Raman spectra of the annealed films deposited with different gas flow ratios

a high Si content (lower ratio NH_3/SIH_4). In addition, the spectra of the films fabricated with $NH_3/SIH_4=0.5–3$ show the broadening of the TO phonon line towards the lower frequency side (the asymmetric line shape), which may be correlated to the effect of phonon confinement and the evidence of the formation of a high density of nanostructured Si [25-27]. For Si-Ncs, peak shifts to smaller wavenumber as a function of decreasing size have been widely reported due to quantum confinement effects [28].

In addition, several Raman peaks from the contribution of the β-Si_3N_4 mode are clearly seen in Fig. 5. The Raman peaks emerging at about 230 cm^{-1}, 620 cm^{-1} and 940 cm^{-1} are assigned to β-Si_3N_4 and attributed to E_{2g} mode according to the crystallographic letters [01-082-0702].

The GIXRD and Raman analysis demonstrate that the films contain simultaneously the hexagonal β-Si_3N_4 phase and Si phase.

Indeed, the crystallization of the silicon nitride, deposited by CVD, under its α and β phases is generally obtained only after annealing at high temperature (≥ 1200° C). Wada et al. [29] prepared α-Si_3N_4 from CVD-deposited silicon nitride by annealing at 1520° C under N_2 for 50 min (1 atm) and β-Si_3N_4 by annealing at 2100 °C for 20 min (80 atm).

Scardera et al. [30–32] reported the crystallization of a multilayer structure composed of an alternation of stoichiometric silicon nitride layers and silicon-rich layers deposited by PECVD. Annealing at 1150° C for 2 h under N_2 caused the appearance of diffraction peaks bound to the α and β crystalline phases of Si_3N_4 in addition to the peaks of crystalline Si corresponding to (111), (220) and (311). However, when the same annealing at 1150 °C was applied to a silicon-rich SiN_x monolayer or to a stoichiometric Si_3N_4 monolayer, none of the two crystalline α and β phases of Si_3N_4 was present. The silicon-rich SiN_x monolayer only exhibited Si nanocrystals and the stoichiometric Si_3N_4 monolayer remained amorphous.

The exception is the study published in 2015 by Torchynska et al. [33]. These authors deposited silicon-rich SiN_x layers by PECVD by varying the ratio of NH_3 and SiH_4 gases from $R=0.56$ to $R=1$. The layers were then annealed under N_2 at 1100 °C for 30 min. X-ray diffraction measurements under grazing incidence have identified the presence of the crystalline phase of β-Si_3N_4 (hexagonal), a SiN_x amorphous phase and an amorphous Si phase.

A brief review of the literature regarding the CVD of layers of SiN_x highlighted by one article Kshirsagar et al. [34] which reports the presence of a β-Si_3N_4 crystalline phase after coating layers by ICP-CVD (inductively coupled plasma CVD) from precursor gases SiH_4, N_2 and Ar, with a ratio $N_2/SiH_4=0.5$ or 1. No post-deposit annealing has been done. According to the authors, the ICP technique provides an activation energy equivalent to that obtained during thermal annealing at 1500–1700 °C.

By combining the Raman spectroscopy and the GIXRD analysis, we have shown the relatively low-temperature formation of β-Si_3N_4 nanocrystals.

It seems that this is the first that we can get the SiN_x phase at this temperature by a rapid annealing.

It is important to determine the energy of the optical band gap (Eg) of a thin-film material, because Eg is essential to exploit the electronic band structure of a material and implements the application of a film in the field of optoelectronics.

3.3 Optical properties

For photovoltaic application, it is necessary to know the optical gaps of the nanostructured layers and adjust these values as a function of crystal fraction and crystal grain size. The optical properties of the thin films were

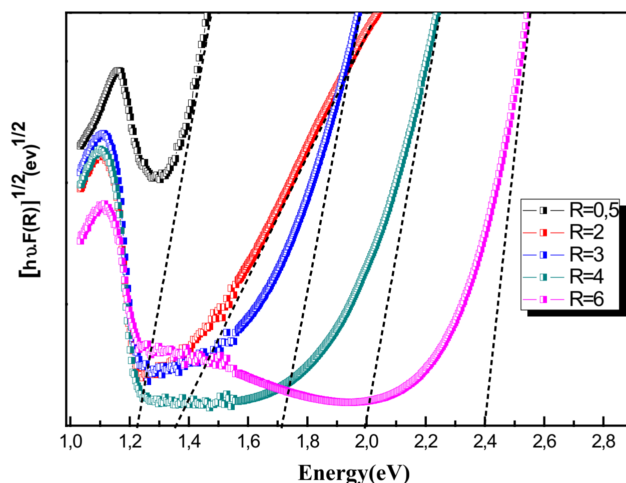

Fig. 6 Indirect optical gap of SiNx with different NH_3/SiH_4

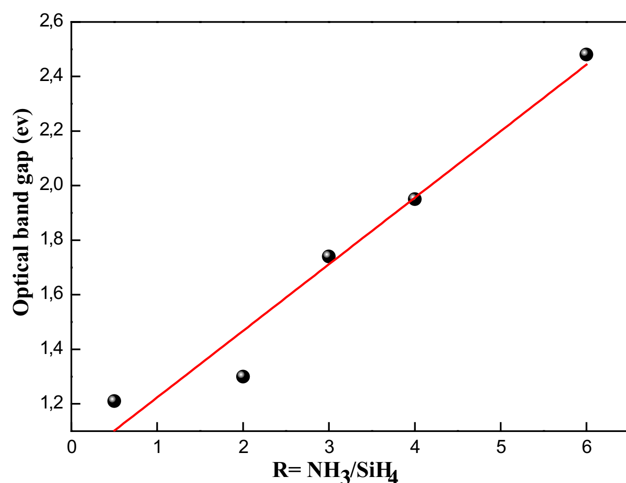

Fig. 7 Evolution of the indirect optical gap with the NH_3/SiH_4 ratio

determined by a spectrophotometer in reflectance mode. The conversion of the reflectance data into absorbance is given by the relationship of Kubelka Munk [35, 36].

The optical band gap (Eg), known as Tauc's gap, is calculated by extrapolation of the linear portion of the curve $(F(R)\ h)^{1/2}$ until zero absorption (h = 0), as β-Si_3N_4 is considered an indirect band dielectric by several works [37–39], shown in Fig. 6. The obtained values are presented in Fig. 7. The results show that the band gap is little bit reduced. Similar results are reported by several authors and attributed the decrease in the gap to the formation of defect states in the forbidden energy gap [40].

When the SiN_x layer is richer in silicon, indicating a decrease in the energy of the optical gap E_g, the latter corresponds to the average gap between that of the Si-Ncs and that of the silicon nitride. The shift of E_g confirms the role of quantum confinement in the luminescence mechanisms of these structures.

As the excess of silicon increases, the size of the nanoparticles increases or the quantum quantification imposes a diminution of the gap when the size increases [41].

The expected decrease in Tauc gap with decreasing R flow (due to the higher Si content) is associated with an increase of the higher absorption due to lower band gap, and a similar increase in the size of Si-Ncs [42].

Generally, the optical band gap of the two-phase network where Si-Ncs are included into the a-SiN_x matrix depends on the proportion and size of Si-Ncs. The optical band gap is governed by the contributions of two parameters E (Si-Ncs) and E (SiN_x) and it is the band gap of the resulting material. The measured gap, therefore, corresponds to the effective gap of the material: it is connected to the atomic ratio N/Si. The optical band gap E (Si-Ncs) of Si-Ncs comes from the optical band interval of c-Si and can increase further due to the quantum confinement effect of Si-Ncs.

The apparition of nanocrystals in amorphous matrix diminishes the density of states and defects and enhances the electrical properties and is very suitable for stable devices as solar cells. Knowing that the minority carrier lifetime, the electron mobility and conductivity are reduced in amorphous silicon nanoparticle [43]. The thermal annealing has not only an effect on the transition from the amorphous to nanocrystalline phase materials but also on photoluminescence where the luminescence property from crystalline particles was found to be more efficient [44]. Moreover, it is important to note also that obtaining β-Si_3N_4 phase seems to be advantageous by several works since they found that the stability order of the three types of polymorphs was β-Si_3N_4 > α-Si_3N_4 > γ-Si_3N_4 [45, 46].

To study the effect of the variation of the chemical structure of the layer on the optical properties, we carried out photoluminescence measurements at room temperature on the different samples. The emission spectra obtained under 325 nm excitation are shown in Fig. 8. They are a superposition of several PL bands. In particular, we observe a shift of the maximum luminescence toward the higher energies when NH_3/SIH_4 increases. Two significant regions appear, one in the blue and the second in the red with several peaks. By analysing nearby, the spectra we obtain decompose into several peaks situated in different ratios. The first (P1) located at 1.47 eV emerges from ratios 0.5 to 2 and decreases in intensity for ratios greater than 2 and reappears timidly at the ratio $NH_3/SIH_4 = 4$. The second peak (P2) is shown in the region 1.8–1.9 eV and grows at $NH_3/SIH_4 = 3$ and up. Another peak (P3) is found around 2.35 eV and is maximum for $NH_3/SIH_4 = 4$. A band (P4) is spread over the 2.6–2.8 eV range, increase in intensity from $NH_3/SIH_4 = 2$ and reaches its maximum at $NH_3/SIH_4 = 4$. Then, it is the band (P5) in the range

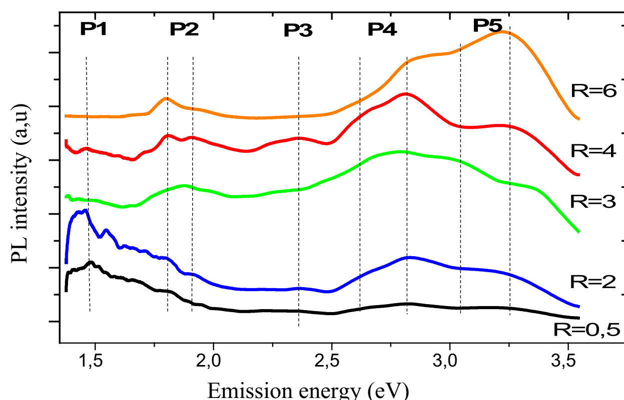

Fig. 8 Room temperature photoluminescence spectra of the 950 °C annealed SiNx films at different ratio

(3.0, 3.2) eV which dominates at $NH_3/SIH_4=6$. These different emissions correspond to several sources that can contribute to luminescence. It was shown in previous work [21] that some bands have shown negligible variations in their PL peak positions with the annealing temperature, it was concluded that these peaks are attributed to radiative recombination from defect-related centers in the SiN_x matrix.

These are the bands corresponding to P4 and P5 and are attributed to recombination via Si dangling bond levels (K°centers) and the nitrogen dangling bond levels (N4 + or N2°), respectively [47, 48].

The emergence of the bands P1, P2 and P3 confirms the results of the formation of grains of different sizes. The P2 band decreases considerably in intensity as the ratio decreases and moves towards the low energies with Si content increasing.

On the basis of the emission energy and the previous simulations that have valued relationships between optical band gap energy and the diameter of Si-QD within the matrix, we can deduce the size of the nanocrystals (d) knowing their luminescence energies.

Several laws model this gap energy variation. Typically, we find a law of the type:

$E^{conf}_{gap}=E^{Si}_{gap}+A/d^{n}$.

With E^{Si}_{gap} close to the gap energy of bulk silicon and n is less than 2. We then find n values of 1.39 [49], 1.78 [50], and even 2 [41], n tends to 2 for larger sizes where the effective mass approximation becomes valid. It is then interesting to compare the sizes results deduced from photoluminescence with simulations of the band gap of Si-Ncs and those determined by XRD experiments.

Considering the PL emission at P1, P2 and P3, which dominates in the red region the ratio $NH_3/SIH_4=2$, 3 and 4, respectively, and the experimental values, given in a range, obtained from the XRD for different crystallographic directions, it might have an idea about the different sizes of existing nanoparticles.

In Table 3, the crystallite sizes obtained from our experiments are compared with those calculated by the simulated equations using a model of quantum confinement, already mentioned.

As a first result, the simulated Si-QD sizes estimated by [49, 50] are in the same order as our experimental results, while the values calculated by Kim seem overrated.

3.4 Electrical properties

Photocurrent (PC) spectroscopy is a characterization technique that provides information on the electronic states and the absorption spectrum of the analysed material. The principle of this technique is based on the generation of carriers caused by the absorption of photons with energy equal to or greater than the gap of the material and which reveals the effects of quantum confinement in Si-Ncs through photon absorption mechanisms.

In the case of Si-Ncs, this technique is particularly interesting since it makes it possible to explore and determine the absorption threshold (and indirectly the gap) associated with the crystallite size distribution. It also allows us to compare the energetic position of the PC absorption bands with the PL emission bands.

To overcome the PC signal associated with the substrate, the measurements were made in lateral transport mode, for which the illumination and the collection of the photogenerated current are between two contact pads. Ohmic aluminum contacts (Al) were deposited by evaporation for the electrical analysis of our samples.

Because the magnitudes of the currents that come from the thin layer are in very distinct ranges of about 10^{-6} (A) for the ratio $NH_3/SiH_4=3$ and 10^{-8} (A) for $NH_3/SiH_4=4$ and 6, and to compare the shape of the photocurrent spectra where the size of PC is different, the spectra were normalized to maximum photocurrent.

In Fig. 9, the difference between the PC spectra of the samples at different ratios is clearly highlighted. This difference is explained by an additional absorption associated with the Si-Ncs thanks to the widening of the gap of the Si caused by the quantum confinement. On the side of high energies of excitation (> 1.6 eV), the additional PC would come from the absorption of photons in the nanocrystals of small size [51, 52].

The analysis of these spectra allows us to notice the existence of a peak of PC at 1.46 eV for the samples $NH_3/SIH_4=2$ and 3 which contain Si-Ncs having the largest sizes and a peak at 1.85 eV for the sample $NH_3/SIH_4=4$. For the samples $NH_3/SIH_4=2$, 3 and 4, the Si-Ncs have a smaller size and the maximum of PC is thus displaced towards the large energies. We note the good agreement between the

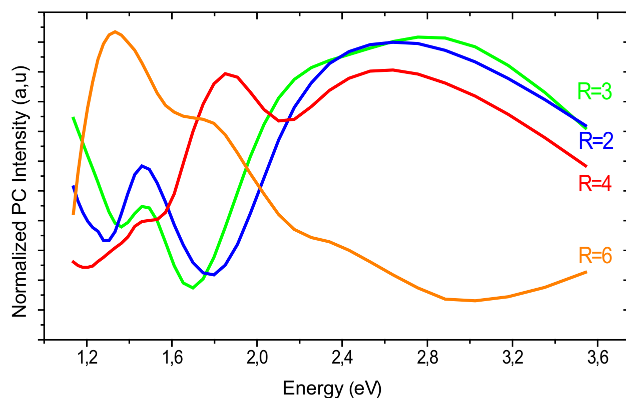

Fig. 9 Normalized photocurrents Spectra taken in lateral configuration of 950 °C annealed samples at different ratio

photocurrent and photoluminescence bands. The best PC response is obtained for SiN_x coatings corresponding to NH_3/SIH_4 values around 3. On the other hand, for the highest ratio $NH_3/SIH_4 = 6$, at high energies the photocurrents are low. The contribution of the composite layer is almost zero and the photogenerated current is mainly due to the absorption in the silicon substrate.

These observations allow assigning the measured photocurrent in these multilayer structures to the generation and transport of photocreated charges in the layers containing Si-Ncs. Finally, the results from photocurrent spectroscopy have clearly demonstrated the existence of an increased absorption on the high energy side associated with Si-Ncs which could be very interesting for the improvement of solar cell efficiency. Si-Ncs form a continuous network and behave similarly to a Si layer and the results of PC allowed us firstly to highlight a photovoltaic effect in the Si-Ncs and secondly to determine the contribution of the Nano composite layer.

4 Conclusion

This work focuses on the realization and characterization of silicon nitride thin layers embedding silicon nanoparticles. Such class of materials receives a lot of attention for the possible application in the new generation of optoelectronic devices.

Amorphous silicon nitride thin films have been deposited using SiH_4 and NH_3 as source gases. The Gas flow ratio NH_3/SiH_4 has significant effect on the structural and optical properties and therefore on the electrical response of the films.

As the silicon content in the SiN_x layer increases, the Nano crystallites size raises and therefore the density of the larger Nano crystallites increases.

The refractive index was shown to increase with the excess of silicon to approach that of c-Si. Progressive reduction in the optical gap occurs with decreasing gas ratio. As the refractive index increase the optical gap varies from 2.4 eV for ratio $NH_3/SIH_4 = 6$ to 1.3 eV for silicon rich SiN_x at $NH_3/SIH_4 = 0.5$.

By modifying the characteristics of the nanostructures such as the size, the degree of crystallinity, it is possible to modify the gap of the nanostructures. Thus it is possible to modify the effective gap of the material by annealing at 950 °C for only 70 s. Annealing at 950 °C has the effect of modifying the properties of the matrix and silicon nanoparticles. Applying a rapid thermal processing key objective is to reduce the crystallization thermal budget without altering the junction and the substrate.

A strong visible photoluminescence (PL) can be observed in silicon nitride and the evolution of photoluminescence with the NH_3/SiH_4 ratio is correlated with the evolution of the structure. The results from photocurrent spectroscopy due to the contribution of the composite layer have clearly demonstrated the existence of an increased absorption on the high energy side associated with Si-Ncs which could be very interesting for the improvement of solar cell efficiency.

We showed on the one hand the relatively low-temperature formation of β-Si3N4 Nano crystals and on the other hand the advantage to obtain a β-Si_3N_4 matrix considered by several works as the most stable phases of Si_3N_4.

This study is a contribution to the understanding of the formation of silicon nanoparticles in a silicon nitride matrix and shows that the integration of nanocrystals into an industrial process is potentially viable.

It would be interesting to test the potential contribution of these silicon nanocrystals embedded in the antireflection coating (ARC) for conventional silicon photovoltaic cells without modifying the basic manufacturing process of the solar cells.

These are the first results we obtained, we applied this process on 4 inch wafers and the electrical results are in progress.

Acknowledgements This work was supported by the "Fond National de la Recherche", DGRSDT/MESRS, Algeria, Ministry of Higher Education and Scientific Research.

References

1. T. Trupke, M.A. Green, P. Würfel, Improving solar cell efficiencies by down-conversion of high-energy photons. J. Appl. Phys. **92**, 1668–1674 (2002)
2. K. Yano, T. Ishii, T. Hashimoto et al., Room-temperature single-electron memory. IEEE T-ED **41**, 1628–1638 (1994)
3. W. Liao, X. Zeng, W. Yao, X. Wen, Photoluminescence and carrier transport mechanisms of silicon-rich silicon nitride light emitting device. Appl. Surf. Sci. **351**, 1053–1059 (2015)

4. P.L. Li, C. Gau, C.W. Liu, Correlation between photo response and nanostructures of silicon quantum dots in annealed Si-rich nitride films. Thin. Solid Films **529**, 185–189 (2013)
5. S. Hong, I.B. Baek, G.Y. Kwak, S.H. Lee, J.S. Jang, K.J. Kim, A. Kim, Improved electrical properties of silicon quantum dot layers for photovoltaic applications. Sol. Energy. Mater. Sol. Cells. **150**, 71–75 (2016)
6. D. Das, D. Kar, Structural studies of n-type nc-Si–QD thin films for nc-Si solar cells. J. Phys. Chem. Solids. **111**, 115–122 (2017)
7. G.R. Lin, Y.H. Pai, C.T. Lin, C.C. Chen, Comparison on the electroluminescence of Si-rich SiNx and SiOx based light emitting Diodes. Appl. Phys. Lett. **96**, 263514 (2010)
8. C.D. Lin, C.H. Cheng, Y.H. Lin, C.L. Wu, Y.H. Pai, G.R. Lin, Comparing retention and recombination of electrically injected carriers in Si quantum dots embedded in Si-rich SiNx films. Appl. Phys. Lett. **99**, 243501 (2011)
9. D. Li, J. Huang, D. Yang, Enhanced electroluminescence of silicon-rich silicon nitride light-emitting devices by NH3 plasma and annealing treatment. Phys. E **41**, 920–922 (2009)
10. G.R. Lin, S.P. Su, C.L. Wu, Y.H. Lin, B.J. Huang, H.Y. Wang, C.T. Tsai, C.I. Wu, Y.C. Chi, Si-rich SiNx based Kerr switch enables optical data conversion up to 12 Gbit/s. Sci. Rep. UK **5**, 9611 (2015)
11. S. Mohammed, M.T. Nimmo, A.V. Malko, C.L. Hinkle, Chemical bonding and defect states of LPCVD grown silicon-rich Si3N4 for quantum dot applications. J. Vac. Sci. Technol. A **32**(2), 021507 (2014)
12. I. Parkhomenkoa, L. Vlasukovaa, F. Komarovb, O. Milchaninb, M. Makhavikoub, A. Mudryic, V. Zhivulkoc, J. Żukd, P. Kopycińskid, D. Murzalinove, Origin of visible photoluminescence from Si-rich and N-rich silicon nitride films. Thin. Solid Films **626**, 70–75 (2017)
13. X. Di Dawei, P.W.Ivan Heli, A.G. Martin, C. Gavin, Optical characterisation of silicon nanocrystals embedded in SiO2/Si3N4 hybrid matrix for third generation photovoltaics. Nanoscale Res. Lett. **6**, 612–618 (2011)
14. G. Conibeer, M. Green, E.-C. Cho, D. König, Y.H. Cho, T. Fangsuwannarak, G. Scardera, E. Pink et al., Silicon quantum dot nanostructures for tandem photovoltaic cells. Thin. Solid Films **516**, 6748–6756 (2008)
15. P.J. Wu, Y.C. Wang, I.C. Chen, Fabrication of Si heterojunction solar cells using P-doped Si nanocrystals embedded in SiNx films as emitters. Nanoscale Res. Lett. **8**(1), 457 (2013)
16. C. Jiang, M.A. Green, Silicon quantum dot superlattices: modeling of energy bands, densities of states, and mobilities for silicon tandem solar cell applications. J. Appl. Phys. **99**, 114902 (2006)
17. R Chaoui, B Mahmoudi, A Messaoud, Y SiAhmed, A Mefoued, B Mahmoudi, Silicon solar cell emitter profile tailoring using the DOSS diffusion technique. 1st Africa Photovoltaic Solar Energy Conference and exhibition. Durban, South Africa, 27–29 March (2014)
18. T.V. Torchynska, L.G. Vega-Macotela, L. Khomenkova, A. Slaoui, Light-emitting mechanism varying in Si-rich-SiNx controlled by film's composition. Adv. Nano. Res. **5**(3), 261–279 (2017)
19. E.D. Palik, *Handbook of Optical Constants of Solids Academic* (Elsevier, New York, 1985), pp. 578–774
20. A.S. Keita, A.E. Naciri, F. Delachat, M. Carrada, G. Ferblantier, A. Slaoui, Spectroscopic ellipsometry investigation of the optical properties of nanostructured Si/SiNx films. J. Appl. Phys. **107**, 093516 (2010)
21. B. Benyahia, F. Tiour, L. Guerbous, R. Chaoui, I. Menous, B. Mahmoudi, A. Mefoued, A. Guenda, Evolution of optical and structural properties of silicon nanocrystals embedded in silicon nitride films with annealing temperature. J. Nano Res. **49**, 163–173 (2017)
22. N. Budini, P.A. Rinaldi, J.A. Schmidt, R.D. Arce, R.H. Buitrago, Influence of microstructure and hydrogen concentration on amorphous silicon crystallization. Thin Solid Films **518**, 5349–5354 (2010)
23. L.V. Mercalo, E.M. Esposito, P.D. Veneri, G. Fameli, First and second-order Raman scattering in Si nanostructures within silicon nitride. Appl. Phys. Lett. **97**, 153112 (2010)
24. A. Kshiragar, P. Nyaupane, D. Bodas, S.P. Duttagupta, S.A. Gangal, Deposition and characterization of low temperature silicon nitride films deposited by inductively coupled plasma CVD. Appl. Surf. Sci. **257**, 5052–5058 (2011)
25. F. Komarov, L. Vlasukova, I. Parkhomenko, O. Milchanina, A. Mudryi, A. Togambaeva, O. Korolik, Raman study of light-emitting SiNx films grown on Si by low-pressure chemical vapor deposition. Thin Solid Films **579**, 110–115 (2015)
26. O. Debieu, R.P. Nalini, J. Cardin, X. Portier, J. Perrière, F. Gourbilleau, Structural and optical characterization of pure Si-rich nitride thin films. Nanoscale Res. Lett. **8**, 31–36 (2013)
27. D.H. Ma, W.J. Zhang, R.Y. Luo, Z.Y. Jiang, Q. Ma, X.B. Ma, Z.Q. Fan, D.Y. Song, L. Zhang, Effects of nitrogen impurities on the microstructure and electronic properties of P-doped Si nanocrystals emebedded in silicon-rich SiNx films. Superlattice. Microst. **93**, 269–279 (2016)
28. S.K. Gupta, P.K. Jha, Modified phonon confinement model for size dependent Raman shift and linewidth of silicon nanocrystals. Solid. State. Commun. **49**, 1989–1992 (2009)
29. N. Wada, S. Solin, J. Wong, S. Prochazka, Raman and IR absorption spectroscopic studies on α, β, and amorphous Si3N4. J. Non-Cryst. Solids. **43**, 7–15 (1981)
30. G Scardera, Correlating structural and optical properties of silicon nanocrystals embedded in silicon nitride: an experimental study of quantum confinement for photovoltaic applications. PhD thesis. UNSW Sydney (Australia) (2008)
31. G. Scardera, T. Puzzer, I. Perez-Wurfl, G. Conibeer, The effects of annealing temperature on the photoluminescence from silicon nitride multilayer structures. J. Cryst. Growth **310**, 3680 (2008)
32. G. Scardera, E. Bellet-Amalric, D. Bellet, T. Puzzer, E. Pink, G. Conibeer, Formation of a Si-Si3N4 nanocomposite from plasma enhanced chemical vapour deposition multilayer structures. J. Cryst. Growth. **310**, 3685 (2008)
33. T.V. Torchynska, J.L. CasasEspinola, L. Khomenkova, E. Vergara Hernandez, J.A. AndracaAdame, A. Slaoui, Structural and light emitting properties of silicon-rich silicon nitride films grown by plasma enhanced-chemical vapor deposition. Mat. Sci. Semicon. Proc. **37**, 46–50 (2015)
34. A. Kshirsagar, P. Nyaupane, D. Bodas, S.P. Duttagupta, S.A. Gangal, Deposition and characterization of low temperature silicon nitride films deposited by inductively coupled plasma CVD. Appl. Surf. Sci. **257**, 5052–5058 (2011)
35. S. Ebraheem, A. El Saied, Band gap determination from diffuse reflectance measurements of irradiated lead borate glass system doped with TiO2 by using diffuse reflectance technique. Mat. Sci. Appl. **4**, 324–329 (2013)
36. B. Karvaly, I. Hevesi, Investigations on diffuse reflectance spectra of V205 PowderZ. Naturforsch **26a**, 245–249 (1971)
37. P. Singh, M.K. Harbola, D.D. Johnson, Better band gaps for wide-gap semiconductors from a locally corrected exchange-correlation potential that nearly eliminates self-interaction errors. J. Phys. Condens. Matter. **29**(42), 424001 (2017)
38. O. Blázquez, J. López-Vidrier, S. Hernández, J. Montserrat, B. Garrido, Electro-optical properties of non-stoichiometric silicon nitride films for photovoltaic applications. Energy Procedia. **44**, 145–150 (2014)
39. V.A. Gritsenko, Electronic structure of silicon nitride. Phys. Uspekhi. **55**(5), 498–507 (2012)

40. R. Hazem, M. Izerrouken, A. Sari, S. Kermadi, M. Msimanga, A. Benyagoub, M. Maaza, M. Belgaid, M. Boumaour, Radiation damage induced by swift heavy ions in TiO2 sol–gel films nanocrystallines. Nucl. Instrum. Methods Phys. Res. B **304**, 16–22 (2013)
41. T.Y. Kim, N.M. Park, K.H. Kim, G.Y. Sunga, Y.W. Ok, T.Y. Seong, C.J. Choi, Quantum confinement effect of silicon nanocrystals in situ grown in silicon nitride films. Appl. Phys. Lett. **85**, 5355–5359 (2004)
42. M.L. Mastronard, F.M. Flaig, D. Faulkner, E.J. Henderson, C. Kübel, U. Lemmer, G.A. Ozin, Size dependent absolute quantum yields for size––separated collodially-stable silicon nanocrystals. Nano. Lett. **12**, 337–342 (2012)
43. P.R.J. Wilson, T. Roschuk, K. Dunn, E.N. Normand, E. Chelomentsev, O.H.Y. Zalloum, J. Wojcik, P. Mascher, Effect of thermal treatment on the growth, structure and luminescence of nitride-passivated silicon nanoclusters. Nanoscale Res. Lett. **6**, 168 (2011)
44. R. Amrani, F. Pichot, L. Chahed, Y. Cuminal, Amorphous-nanocrystalline transition in silicon thin films obtained by argon diluted silane PECVD. Cryst. Struct. Theor. Appl. **1**, 57–61 (2012)
45. B.H. Yu, D. Chen, First-principles study on the electronic structure and phase transition of α, β and γ-Si3N4. Acta. Phys. Sin. **61**, 197102 (2012)
46. L. Cui, M. Hu, Q. Wang, Y. Yang, Prediction of novel hard phases of Si3N4: first-principles calculations. J. Solid. State. Chem. **228**, 20–26 (2015)
47. B.H. Kim, C.H. Cho, T.W. Kim, N.M. Park, G.Y. Sung, S.J. Park, Photoluminescence of silicon quantum dots in silicon nitride grown by NH3 and SiH4. Appl. Phys. Lett. **86**, 091908 (2005)
48. T. Torchynska, L. Khomenkova, A. Slaoui, Modification of Light emission in si-rich silicon nitride films versus stoichiometry and excitation light energy. J. Electron. Mat. **47**(7), 3927–3933 (2018)
49. C. Delerue, G. Allan, M. Lannoo, Theoretical aspects of the luminescence of porous silicon. Phys. Rev. B. **48**, 11024–11036 (1993)
50. C.L. Wu, G.R. Lin, Inhomogeneous linewidth broadening and radiative lifetime dispersion of size dependent direct bandgap radiation in Si quantum dot. Aip. Adv. **2**, 042162 (2012)
51. J. De la Torre, A. Souifi, A. Poncet, G. Bremond, G. Guillot, B. Garrido, J.R. Morante, Ground and first excited states observed in silicon nanocrystals by photocurrent technique. Solid. State Electron. **49**(7), 1112–1117 (2005)
52. R. Zhang, X.Y. Chen, K. Zhang, W.Z. Shen, Photocurrent response of hydrogenated nanocrystalline silicon thin films. J. Appl. Phys. **100**(10), 104310 (2006)

Publisher's Note Springer Nature remains neutral with regard to jurisdictional claims in published maps and institutional affiliations.